Electronic structures of a diagonally striped lattice: Multiple ($N - 1$)-fold degenerate flat bands

Xiaojuan Ni,[1] Jinli Yan ®,[2] and Feng Liu ®[1,*]

[1]*Department of Materials Science and Engineering, University of Utah, Salt Lake City, Utah 84112, USA*
[2]*School of Computational Science and Engineering, Georgia Institute of Technology, Atlanta, Georgia 30332, USA*

We investigate the electronic structure of an interesting two-dimensional (2D) diagonally striped lattice (DSL). It consists of arrays of N different types of "atoms" or "molecules" with a fixed sequence in both horizontal and vertical directions. Using a tight-binding model, we show that the DSL ($N > 2$) has the symmetry group *Amm*2 and *Pmm*2, and exhibits an oscillatory metallic and insulating phases for the odd- and even-N number, respectively. Some conventional 2D lattices, such as the Lieb lattice, can be related to the derivative DSL via vacancy formation by removing one type of atom in every other ($N - 1$) row of the original DSL. Interestingly, there are multiple ($N - 1$)-fold degenerate flat bands in one group of the derivative DSLs, which affords a unique platform for studying many-body physics. In addition to atomic and molecular lattices, we suggest other artificial DSLs, such as photonic and phononic, to be also constructed with possibly interesting properties.

I. INTRODUCTION

Two-dimensional (2D) lattices have been an intriguing subject, since it lays the foundation for many fields of research in physics. Despite their seemingly simple structure, they can exhibit very rich electronic properties and exotic physical phenomena [1–3]. For instance, the fascinating Dirac bands in honeycomb lattice of graphene [4–7] and exotic flat bands (FBs) in Kagome and Lieb lattices [8–12] have attracted an ever-increasing interest during the last decades. Various quantum phenomena may be derived from electronic band structures and interactions in 2D lattices, such as nontrivial topology associated with Dirac bands and FBs [4,5,8,13–20], magnetism, and superconductivity derived from many-body interactions [21–24].

In this work, the two-dimensional diagonally striped lattice (DSL) is introduced. It represents a square lattice made of a designated pattern of N different colors, arranged in a fixed sequence in both horizontal and vertical directions. Alternatively, one can also view the pattern being formed by repeatedly stacking a row of an N-color sequence but shifting the color by one position in every row. One wonders what would be the electronic band structure of this array if different colors were turned into different types of atoms? For the simplest case of $N = 2$, one immediately realizes that it is simply a checkerboard lattice. But what if $N > 2$? And what happens if some of the atoms in such a lattice are missing?[1]

Using a tight-binding (TB) model, we have systematically investigated the evolution of band structures of the original and derivative (i.e., with missing rows) DSLs as a function of N. The DSL ($N > 2$) has the symmetry group of *Amm*2 and *Pmm*2 for the odd- and even-N lattices, respectively. They are found to exhibit an interesting odd-even oscillation of metallic-insulating phase with respect to N, similar to atomic chains due to quantum size effect [26]. For the derivative DSL, modified by removing one type of atom in every other ($N - 1$) row, when $N = 2$, it reduces naturally to the well-known Lieb lattice, which is characterized with a FB crossing the Dirac point of two Dirac bands. Interestingly, however, multidegenerated FBs are found to persist in all the derivative DSLs, showing a distinctive FB degeneracy of 1 for odd N but of ($N - 1$) for even N. The multiple ($N - 1$)-fold degenerate flat bands are especially intriguing in terms of topological and many-body physics.

The paper is organized as follows. In Sec. II, we introduce the DSL structure and construction of the TB model. The electronic band structures of the original and derivative DSLs are discussed in Sec. III. We end with a brief summary in Sec. IV.

II. DIAGONALLY STRIPED LATTICE AND TIGHT-BINDING MODEL

The DSL is constructed by shifting an array of N different types of "atoms" or "molecules" with fixed sequence one position to the right for each row in 2D plane, so that the diagonal sites have the same atoms or molecules. Their lattice structures are shown in Figs. 1(a) to 1(h) for $N = 2$ to 9, respectively. Sites *1* to N are indicated by different colors from blue to red. Since the fourfold rotational symmetry in DSL is broken when $N > 2$, the primitive unit cell of DSL is no longer a square but a rectangle, as indicated by the red rectangles in Fig. 1. The first Brillouin zone (1st BZ) of the

---

[1]The idea came out during a trip by one of the authors (F.L.) when he visited the famous historical site Mogao Caves in the Gansu province of China. In Cave No. 204, a fresco of colored Bodhisattva paintings attracted his attention, which consists of the above-mentioned pattern of colors (see Fig. S1 in the Supplemental Material) [25].
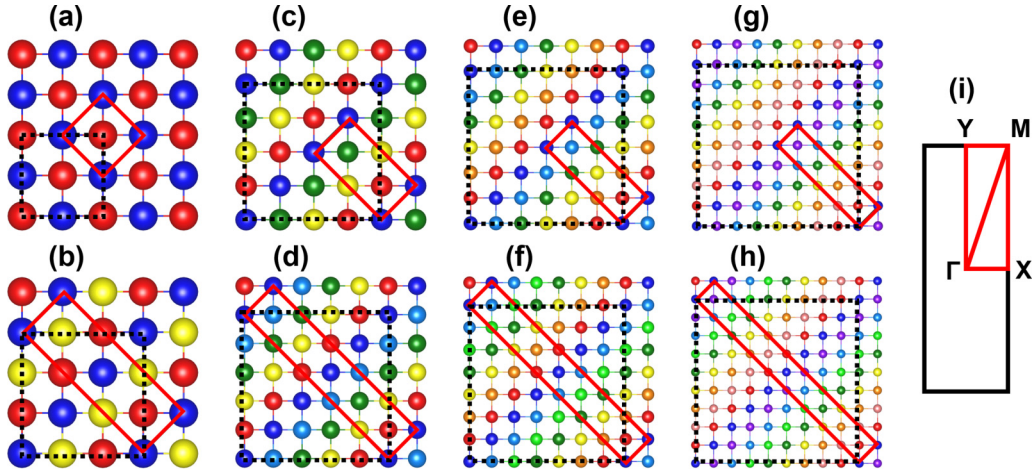
FIG. 1. The DSL structures of (a) $N = 2$, (b) $N = 3$, (c) $N = 4$, (d) $N = 5$, (e) $N = 6$, (f) $N = 7$, (g) $N = 8$, and (h) $N = 9$, respectively. The red rectangle indicates the primitive unit cell and the dashed black square indicates the conventional unit cell. Sites 1 to N are indicated by different colors from blue to red. (i) The first Brillouin zone of DSL.

DSL is shown in Fig. 1(i). The space groups of DSLs are listed in Table I, which are $Amm2$ and $Pmm2$ for odd and even N number, respectively.

We consider the TB Hamiltonian with single-orbital hopping on each lattice site as

$$H = \sum_{i} \varepsilon_i c_i^\dagger c_i + \sum_{\langle i,j \rangle} (t c_i^\dagger c_j + \text{H.c.}), \qquad (1)$$

where ε_i is the on-site energy; $c_i^\dagger$ and c_i are the creation and annihilation operators of an electron on site i, respectively. t represents the hopping between the nearest neighbors (NN) $\langle i, j \rangle$. Electron-electron interaction is not included. The details of TB Hamiltonians for DSL of $N = 2$, 3, and 4 are provided in Appendix A.

III. BAND STRUCTURES OF DSL

In this section, we first present the band structures of the original DSL as a function of N in Sec. III A, which show an oscillatory metallic and insulating phases for odd and even N, respectively. The physical origin of the odd-even oscillation is analyzed in Sec. III B. In Sec. III C, the exceptional DSLs with special lattice energy parameters that exhibit semimetal phase are discussed. Lastly, we present the band structures of the derivative DSL in Sec. III D, and discuss the origin of multiple $(N-1)$-fold degenerate FBs in Sec. III E.

A. Band structures of the original DSL

If the on-site energy of all lattice sites and the NN hopping integrals are the same, the band structures for any DSL with $N > 1$ are nothing but the folded bands of a simple square lattice ($N = 1$), which will not be interesting but are shown in Figs. 2(a) to 2(d) with $N = 3$, 5, 7, and 9, respectively, as reference for comparison. Note that there is a partial FB along Y-M and M-X at the Fermi level, which corresponds to bands in the simple square lattice along X-Y (see Appendix B), by unfolding the bands [27]. To distinguish the lattice sites, the on-site energy difference is introduced. The band structures of DSL with different on-site energies are shown in Figs. 2(e) to 2(h) for $N = 3$ to 9, which all exhibit a metallic behavior.

The band structures of DSLs with even $N = 2$, 4, 6, and 8 are shown in Figs. 3(a) to 3(d) for the case of same on-site energy. Note that without on-site energy difference, the unit cells of lattices of $N = 3$ and 6 are the same, resulting in the same band structure, as shown in Fig. 2(a) and Fig. 3(c). Again, there is a partial FB along a specific k path, which is overlapped with the k path of X-Y in the 1st BZ of the simplest square lattice (see Appendix B). Those band structures for different on-site energies are shown in Figs. 3(e) to 3(h), respectively, which all exhibit an insulating behavior. Therefore, there exists an odd-even oscillation of metallic-insulating phases with respect to N in the original DSLs.

TABLE I. The space group of DSL of different N.

N	No.	Point group	Hermann-Mauguin notation	Schoenflies notation
1	221	$4/m\bar{3}/m$	$Pm\bar{3}m$	$\Gamma_c O_h^1$
2	123	$4/m2/m2/m$	$P4/mmm$	$\Gamma_q D_{4h}^1$
3, 5, 7, 9	38	$mm2$	$Amm2$	$\Gamma_o^b C_{2v}^{14}$
4, 6, 8	25	$mm2$	$Pmm2$	$\Gamma_o C_{2v}^1$
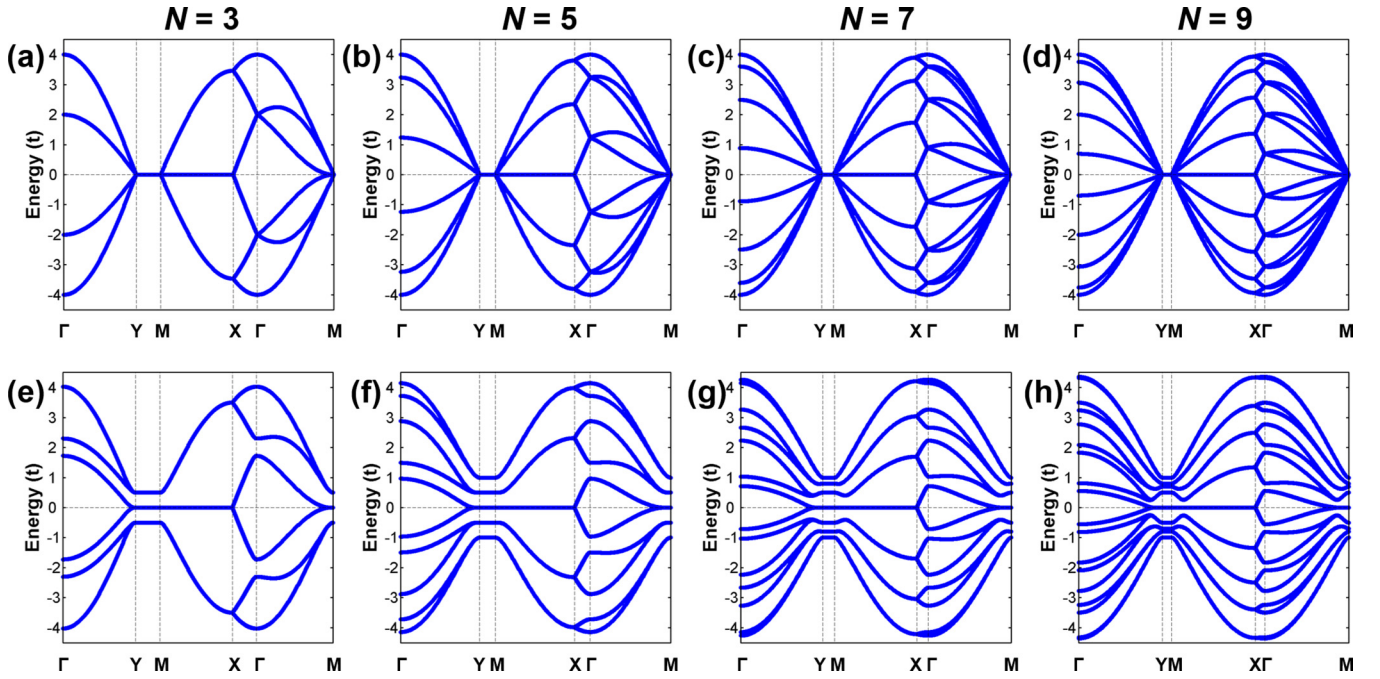
FIG. 2. The band structures of DSL of odd N: (a) $N = 3$, (b) $N = 5$, (c) $N = 7$, (d) $N = 9$ with the same on-site energy ($\varepsilon = 0$), (e) $N = 3$ with $\varepsilon_1 = 0.5$ $\varepsilon_2 = 0.0$ and $\varepsilon_3 = -0.5t$, (f) $N = 5$ with $\varepsilon_1 = 1.0$ $\varepsilon_2 = 0.5$ $\varepsilon_3 = 0.0$ $\varepsilon_4 = -0.5$, and $\varepsilon_5 = -1.0t$, (g) $N = 7$ with $\varepsilon_1 = 1.0$ $\varepsilon_2 = 0.8$ $\varepsilon_3 = 0.5$ $\varepsilon_4 = 0.0$ $\varepsilon_5 = -0.5$, $\varepsilon_6 = -0.8$, and $\varepsilon_7 = -1.0t$, and (h) $N = 9$ with $\varepsilon_1 = 1.0$ $\varepsilon_2 = 0.8$ $\varepsilon_3 = 0.7$ $\varepsilon_4 = 0.5$ $\varepsilon_5 = 0.0$ $\varepsilon_6 = -0.5$, $\varepsilon_7 = -0.7$, $\varepsilon_8 = -0.8$, and $\varepsilon_9 = -1.0t$, respectively.

B. Odd-even oscillation of metallic-insulating phases

To better understand the odd-even oscillation of metallic-insulating phases with respect to N, we have analyzed the wave functions at a specific k point in the lattice of $N = 3$

and 4. There are six bands in the primitive unit cell of $N = 3$ lattice with the band index 1 to 6 from the valence to conduction bands [see Figs. 2(a) and 2(e)]. Without on-site energy difference, all sites contribute equally to the six
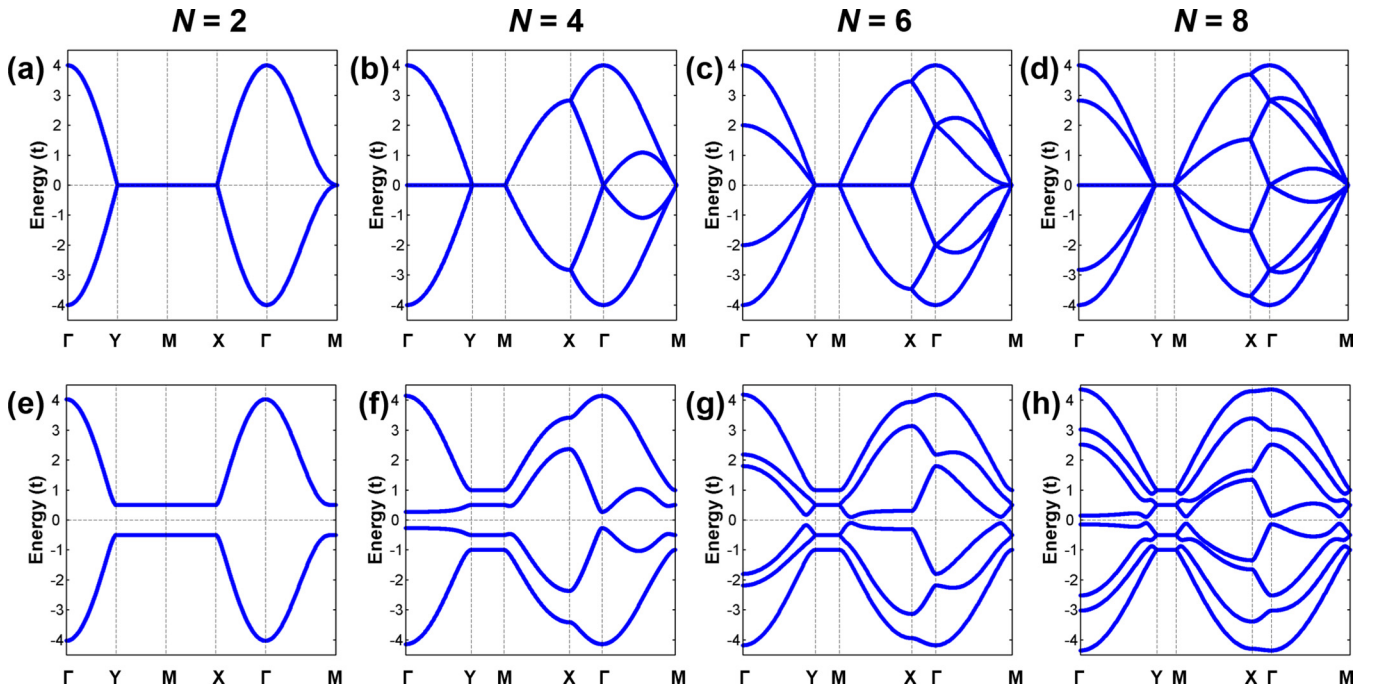
FIG. 3. The band structures of DSL of even N: (a) $N = 2$, (b) $N = 4$, (c) $N = 6$, (d) $N = 8$ with the same on-site energy ($\varepsilon = 0$), (e) $N = 2$ with $\varepsilon_1 = 0.5$ and $\varepsilon_2 = -0.5t$, (f) $N = 4$ with $\varepsilon_1 = 1.0$ $\varepsilon_2 = 0.5$ $\varepsilon_3 = -0.5$, and $\varepsilon_4 = -1.0t$, (g) $N = 6$ with $\varepsilon_1 = 1.0$ $\varepsilon_{2,3} = 0.5$, $\varepsilon_{4,5} = -0.5$, and $\varepsilon_6 = -1.0t$, and (h) $N = 8$ with $\varepsilon_{1,2} = 1.0$, $\varepsilon_{3,4} = 0.5$, $\varepsilon_{5,6} = -0.5$, $\varepsilon_{7,8} = -1.0$ t, respectively.
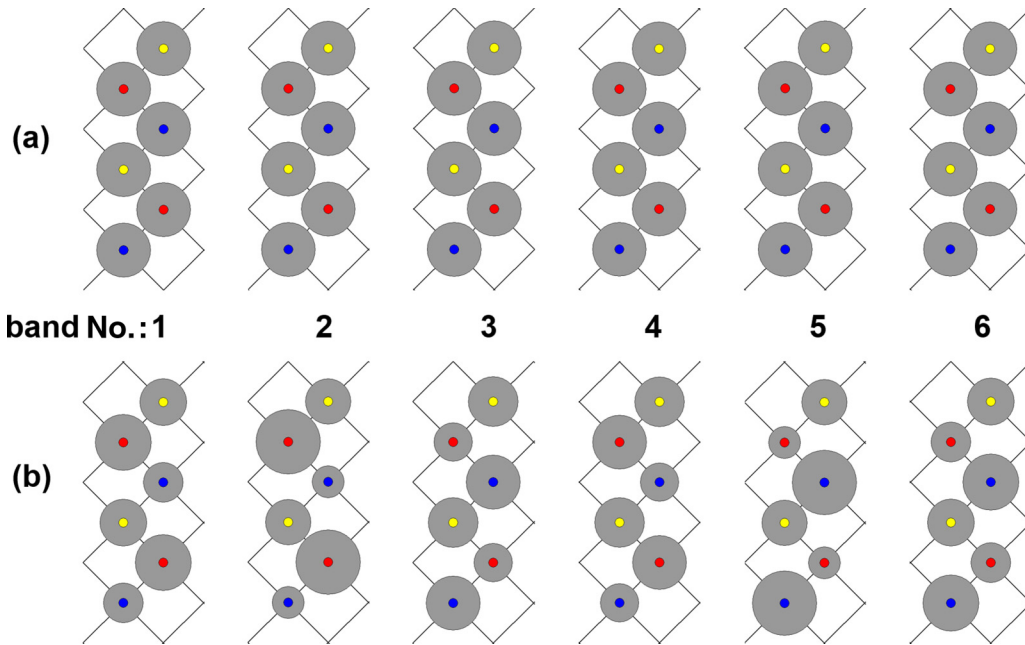
FIG. 4. The wave functions of DSL of $N = 3$ at a specific k point along Γ-M in Figs. 2(a) and 2(e). (a) Without on-site energy difference. (b) Three sites with different on-site energy: $\varepsilon_1 = 0.5$ (blue), $\varepsilon_2 = 0.0$ (yellow), and $\varepsilon_3 = -0.5t$ (red), as indicated by the colors. The numbers represent the band index in the band structures in Figs. 2(a) and 2(e) from valence to conduction bands. The size of the gray dot indicates the magnitude of the wave function.

bands, as shown in Fig. 4(a), which is also indicated by the analysis of eigenvectors in Appendix A. With on-site energy difference, as shown in Fig. 4(b), the valence bands (1 and 2) are predominantly contributed by the sites with negative on-site energy of $\varepsilon_3 = -0.5t$ (red), and the conduction bands (5 and 6) mainly come from the sites with positive energy of $\varepsilon_1 = 0.5t$ (blue), while the yellow sites with $\varepsilon_2 = 0.0$ contribute nearly equally to all bands. In $N = 4$ lattice, there are four bands with band index of 1 to 4 from valence to conduction bands [see Figs. 3(b) and 3(f)]. Without the on-site energy difference, the wave functions of four bands, as shown in Fig. 5(a), again show that these four sites contribute equally to each band (see Appendix A). On the contrary, the wave functions of the four bands in the lattice with on-site energy difference display a distinctively different feature, as shown in Fig. 5(b). Band No. 1 mainly comes from the sites with negative on-site energy of $\varepsilon_3 = -0.5$ (yellow) and $\varepsilon_4 = -1.0t$ (red), while band No. 4 is predominantly contributed by the sites with positive on-site energy of $\varepsilon_1 = 1.0$ (blue) and $\varepsilon_2 = 0.5t$ (green). Bands No. 2 and No. 3 mainly come from the green and yellow site with $\varepsilon_2 = 0.5$ and $\varepsilon_3 = -0.5t$, respectively.

Since we are considering the situation of half filling, then the Fermi level will be always located in the middle of the bands under the conditions of $\varepsilon_i + \varepsilon_{N-i+1} = 0$. Then the origin of the odd-even oscillation of metallic-insulating phase can be easily understood by the appearance of nonbonding state at the Fermi level, similar to the quantum size effect in atomic chains [26]. When N is odd, there is always a nonbonding state at the Fermi level, rendering the system metallic, while when N is even, there is a gap between the bonding

valence bands and antibonding conduction bands without the nonbonding states, rendering the system insulating or semiconducting. In other words, for odd N, there is always one eigenstate of $\varepsilon_{(N+1)/2} = 0$ sitting at the Fermi level and others
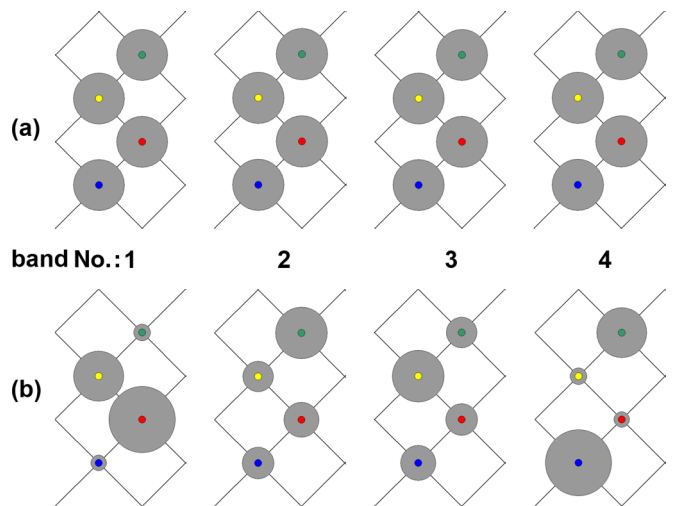
FIG. 5. The wave functions of DSL of $N = 4$ at a specific k point along Γ-M in Figs. 3(b) and 3(f). (a) Without on-site energy difference. (b) Four sites with different on-site energy: $\varepsilon_1 = 1.0$ (blue), $\varepsilon_2 = 0.5$ (green), $\varepsilon_3 = -0.5$ (yellow), and $\varepsilon_4 = -1.0t$ (red), as indicated by the colors. The numbers represent the band index in the band structures in Figs. 3(b) and 3(f) from valence to conduction bands. The size of the gray dot indicates the magnitude of the wave function.
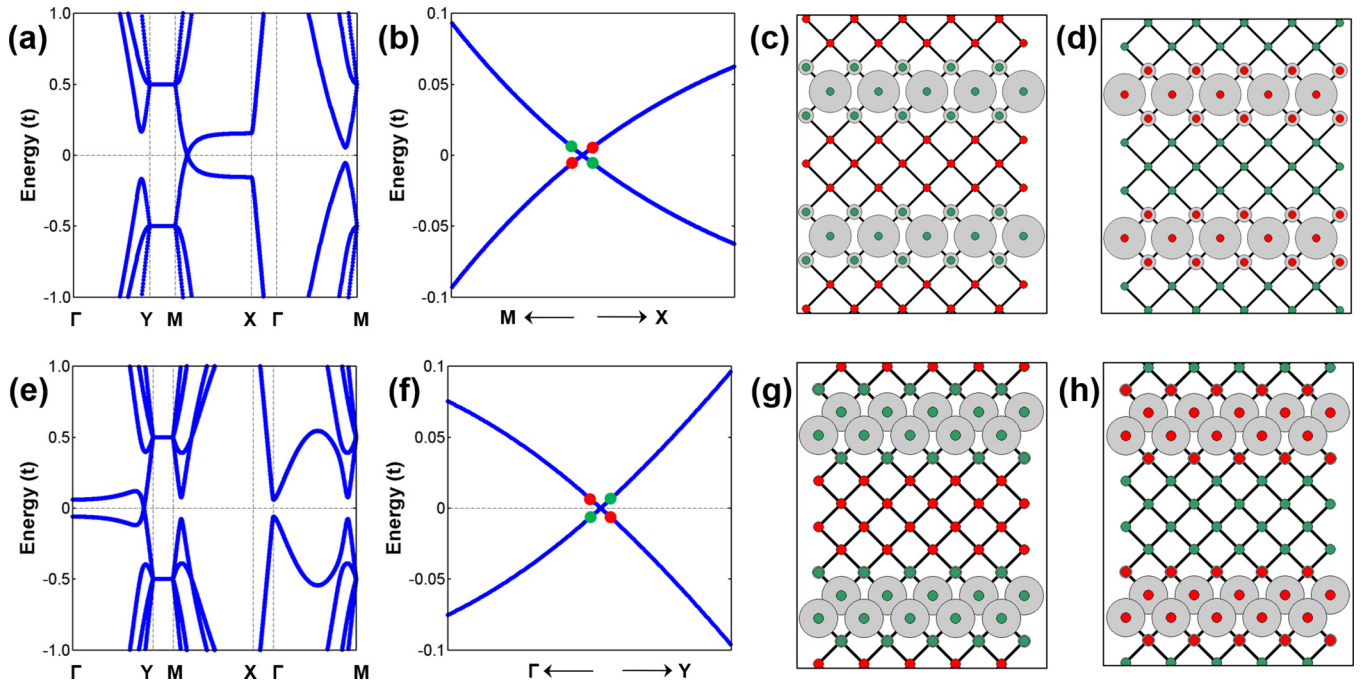
FIG. 6. The band structures of DSL: (a) $N = 6$ with $\varepsilon_{1,2,3} = 0.5$ and $\varepsilon_{4,5,6} = -0.5t$, (d) $N = 8$ with $\varepsilon_{1,2,3,4} = 0.5$ and $\varepsilon_{5,6,7,8} = -0.5t$. (b), (f) Zoom-in band structures around the Dirac point in (a) and (d). (c), (d) Wave functions of the states marked by the green dots in (b) and (f). (d), (h) Wave functions of the states marked by the red dots in (b) and (f). The sites with on-site energy of 0.5 and $-0.5\ t$ are represented by the green and red colors. The size of the light gray dot indicates the magnitude of wave function.

either above or below the Fermi level; for even N, no eigenstate has zero energy and half states above and half below the Fermi level.

C. Semimetal phase in exceptional DSL

Interestingly, in those lattices of even N ($N \geqslant 6$), if the neighboring half N sites have the same magnitude of on-site
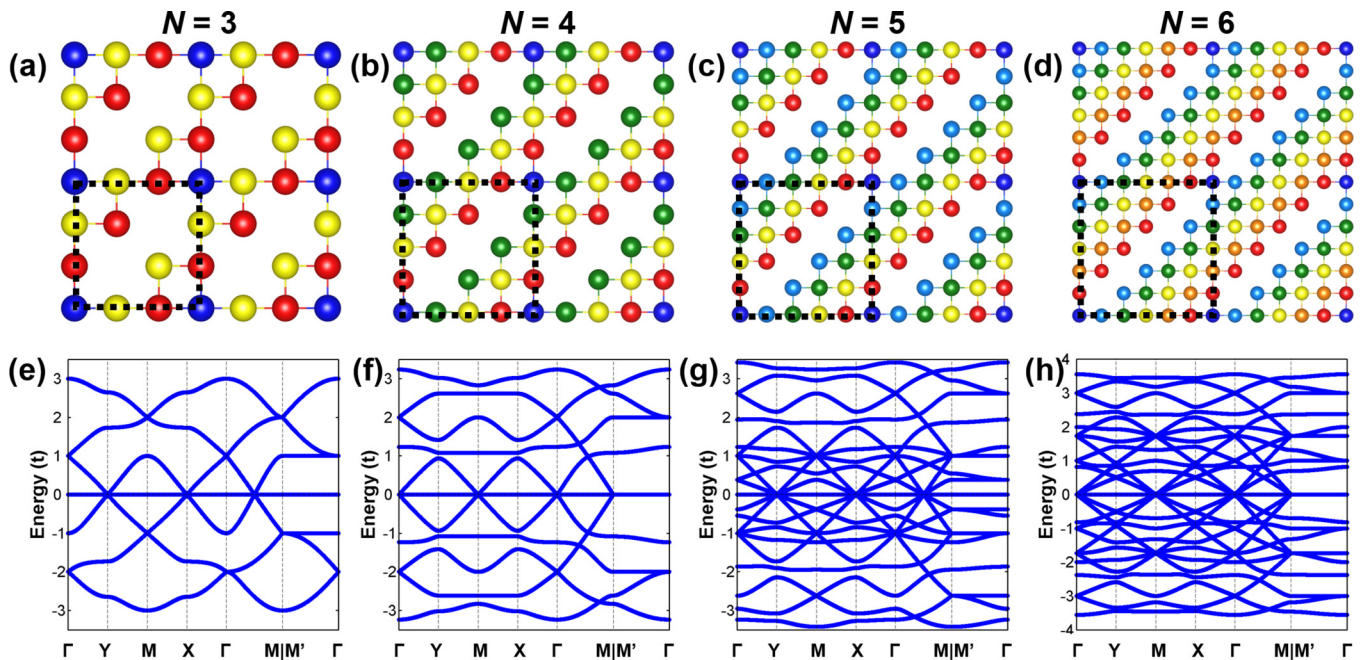
FIG. 7. The structure of the derivative DSL of (a) $N = 3$, (b) $N = 4$, (c) $N = 5$, and (d) $N = 6$, and the corresponding band structures in (e) to (h), respectively. All sites have the same on-site energies. The black dashed square indicates the unit cell. Site 1 to N can be distinguished by the colors from blue to red.
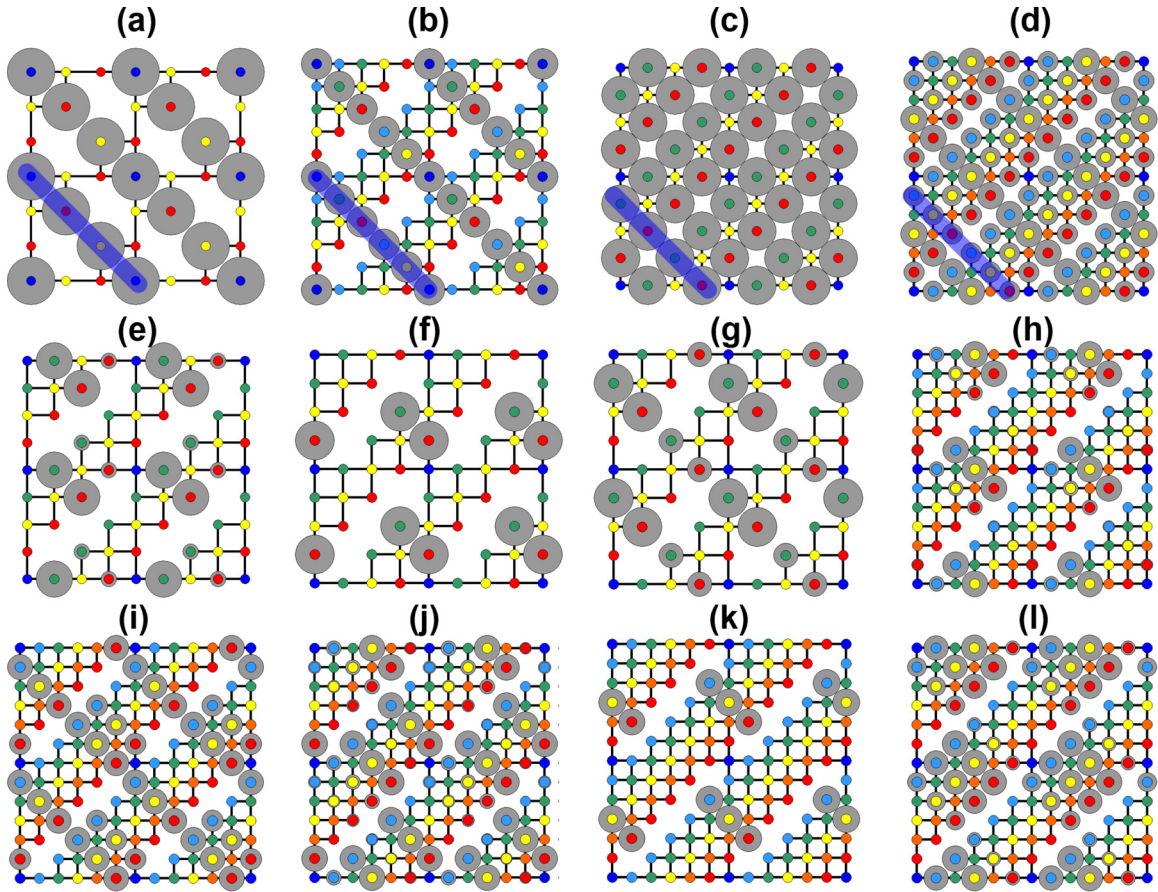
FIG. 8. Wave functions of FBs in a 2-by-2 superlattice of (a) $N = 3$, band index 4, (b) $N = 5$, band index 11, (c) $N = 4$, band index 6 to 8, and (d) $N = 6$, band index 14 to 18. The wave functions of three FBs in lattice of $N = 4$: band index (e) 6, (f) 7, and (g) 8. The wave functions of five FBs in lattice of $N = 6$: band index (h) 14, (i) 15, (j) 16, (k) 17, and (l) 18.

energy as the other half but have the opposite sign, i.e., $\varepsilon_i + \varepsilon_{N-i+1} = 0$, and $|\varepsilon_i| = |\varepsilon_j| \neq 0$, their band structures show a semimetal behavior with a Dirac point, as shown in Fig. 6. The Dirac point in the lattice of $N = 6$ is located along the k path of M-X, which is originated from the partial FB in Fig. 3(c). The wave functions of the states near the Dirac points, as marked by the green and red dots in Fig. 6(b) for $N = 6$, are shown in Figs. 6(c) and 6(d), respectively. The dominant contribution to one set of states near the Dirac point is from the center of the sites (green) with positive on-site energy, and that to the other set of states is from the center of the sites (red) with negative on-site energy. Similarly, for $N = 8$, the Dirac point is located along the k path of Γ-Y, which is originated from the partial FB in Fig. 3(d) as shown in Figs. 6(e) to 6(h). Compared with the wave-function plots (see Appendix C) of the original partial FB in Figs. 3(c) and 3(d), it indicates that the unique on-site energy pattern in this exceptional DSL breaks the degeneracy of the original FB in such a way that two partial FBs are tilted in opposite directions to form the Dirac point.

D. Band structures of derivative DSL

Lastly, we discuss the electronic structures of one specific class of derivative DSLs formed by creating vacancies. One interesting observation is that for $N = 2$, by removing the

atom in the center, the DSL reduces to the well-known Lieb lattice (see Appendix D). Systematically, one may remove one type of atom in every other $(N - 1)$ row of the original DSL, as shown in Figs. 7(a) to 7(d) for $N = 3$, 4, 5, and 6, respectively, to derive a series of Lieb-like lattice of different sizes. Assuming identical on-site energy on all sites, the band structures for lattices with $N = 3$ to 6 are shown in Figs. 7(e) to 7(h). When $N \geqslant 2$, a global FB always exists at the Fermi level just like the Lieb lattice. Interestingly, it is found that for odd N, there is only one single FB; while for even N, there are $(N - 1)$ degenerate FBs at the Fermi level.

E. Multiple $(N - 1)$-fold degenerate flat bands

To better understand the FB in the derivative DSL of large $N > 2$, we have calculated the analytical solutions of the eigenstates of the derivative DSLs of $N = 3$ and 4, with the focus on zero eigenvalue and the corresponding eigenvectors (see Appendix E). The wave functions of FBs at a specific k point $(0,1)$ are shown in Fig. 8. All the sites contributing to the FB locate along the diagonal chains of equal spacing. In the lattices of $N = 3$ and 5, only one FB at the Fermi level, the wave-function plots indicate the electronic states forming the FB are coming from the diagonal sites, as indicated by the thick blue lines in Figs. 8(a) and 8(b). In lattices of $N = 4$ and 6, there are three and five FBs at the Fermi level,

respectively. The wave functions of the multidegenerated FBs are shown in Figs. 8(c) and 8(d), which are contributed from the sites in an alternating pattern in the same row. The wave functions for each individual FB are also shown in Figs. 8(e) to 8(g) with band index 6 to 8 for the case of $N = 4$, and Figs. 8(h) to 8(l) with band index 14 to 18 for $N = 6$. It shows that the FB states for even N are also contributed from the diagonal sites, same as the case of odd N, as indicated by the thick blue lines in Figs. 8(c) and 8(d).

In the unit cell of the lattice of odd N, there is only one equal-spaced chain forming by the diagonal sites, while in contrast, there are $(N - 1)$ such chains in the lattice of even N. Interestingly, the degeneracy of FBs equals to the number of equal-spaced chains in all the lattices with either odd or even N. The condition to have the FB with $(N - 1)$ degeneracy in the lattice of $N = 4$ is $(\varepsilon_2 + \varepsilon_4) = 2\varepsilon_3$; ε_1 can be any value since site 1 (blue) has no contribution to FBs. In order to have the FB located at the Fermi level, ε_3 is set to 0. For odd $N = 3$, the FB locates at the Fermi level with the conditions of $(\varepsilon_1 + \varepsilon_3) = 2\varepsilon_2$ and $\varepsilon_2 = 0$. The conditions to have FBs become even more complicated in the derivative DSL of large N, which are not discussed here.

For comparison, the single-degenerated FB in the original and extended Lieb [28–30] lattices is relatively well understood, while the origin of multidegenerated FBs in the derivative DSLs we found here is less clear. Usually, the flat band is characterized with a compact localized real-space wave function on a plaquette as shown for Kagome and Lieb lattices [11,31]; however, we have not been able to construct such wave functions for the derivative DSLs for $N > 3$. Therefore, the underlying formation mechanism as well as physical properties of the multidegenerated FBs in the derivative DSLs remain to be further explored. We also note that beyond the atomic and molecular lattices, other artificial, such as photonic and phononic, DSLs may also be constructed with possibly interesting properties. For example, the photonic derivative DSL can be constructed to achieve the localized FB states, which have been observed in both photonic Lieb and Kagome lattices formed by an array of optical waveguides [32–35]. In the photonic DSL, the sites can be replaced by the optical waveguides. The on-site energy can be tuned by the refractive index or the radius of the waveguides.

IV. CONCLUSION

In conclusion, we have introduced a class of 2D lattices, the DSL. Using the tight-binding model, we have investigated systematically the electronic band structures of DSLs as a function of lattice size. They are found to exhibit an oscillatory metallic and insulating phases for odd- and even N
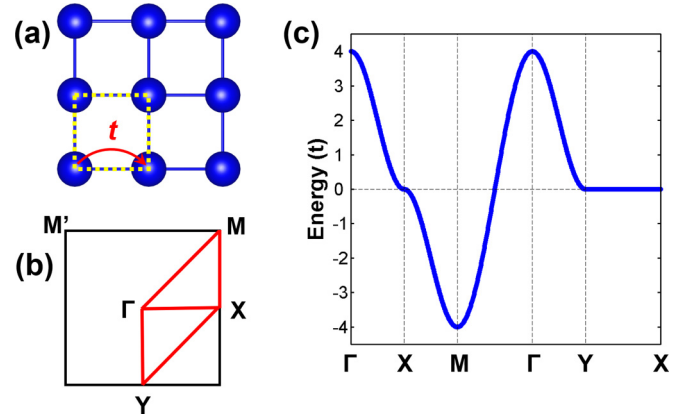
FIG. 9. (a) The simple square lattice. The dashed square indicates the unit cell. The NN hopping is indicated by t. (b) The first Brillouin zone of square lattice. (c) The band structure of the simple square lattice.

number of lattice periodicity, respectively. Dirac bands may exist in some exceptional DSLs having special symmetry of on-site-energy patterns, while flat bands with distinctive degeneracy may exist in one class of derivative DSLs formed by removing one type of atom in every other $(N - 1)$ row of the original DSL. The finding of multiple $(N - 1)$-fold flat bands in derivative DSLs is highly intriguing, which will likely draw immediate attention especially from the field of many-body physics.

APPENDIX A: TB HAMILTONIANS FOR DSLS OF $N = 2$, 3, and 4

The TB Hamiltonian for DSL of $N = 2$ is

$$H = \begin{pmatrix} \varepsilon_1 & 2t(\cos k_x + \cos k_y) \\ 2t(\cos k_x + \cos k_y) & \varepsilon_2 \end{pmatrix}, \quad (A1)$$

which gives two bands

$$E_{1,2}(\vec{k}) = \frac{1}{2}(\varepsilon_1 + \varepsilon_2 \pm \sqrt{(\varepsilon_1 - \varepsilon_2)^2 + 16t^2(\cos k_x + \cos k_y)^2}). \quad (A2)$$

The TB Hamiltonian for DSL of $N = 3$ without on-site energy difference is

$$H = t * \begin{pmatrix} 0 & e^{-ik_1} + e^{-ik_2} & 0 & 0 & 0 & e^{ik_1} + e^{ik_2} \\ e^{ik_1} + e^{ik_2} & 0 & e^{-ik_1} + e^{-ik_2} & 0 & 0 & 0 \\ 0 & e^{ik_1} + e^{ik_2} & 0 & e^{-ik_1} + e^{-ik_2} & 0 & 0 \\ 0 & 0 & e^{ik_1} + e^{ik_2} & 0 & e^{-ik_1} + e^{-ik_2} & 0 \\ 0 & 0 & 0 & e^{ik_1} + e^{ik_2} & 0 & e^{-ik_1} + e^{-ik_2} \\ e^{-ik_1} + e^{-ik_2} & 0 & 0 & 0 & e^{ik_1} + e^{ik_2} & 0 \end{pmatrix}. \quad (A3)$$
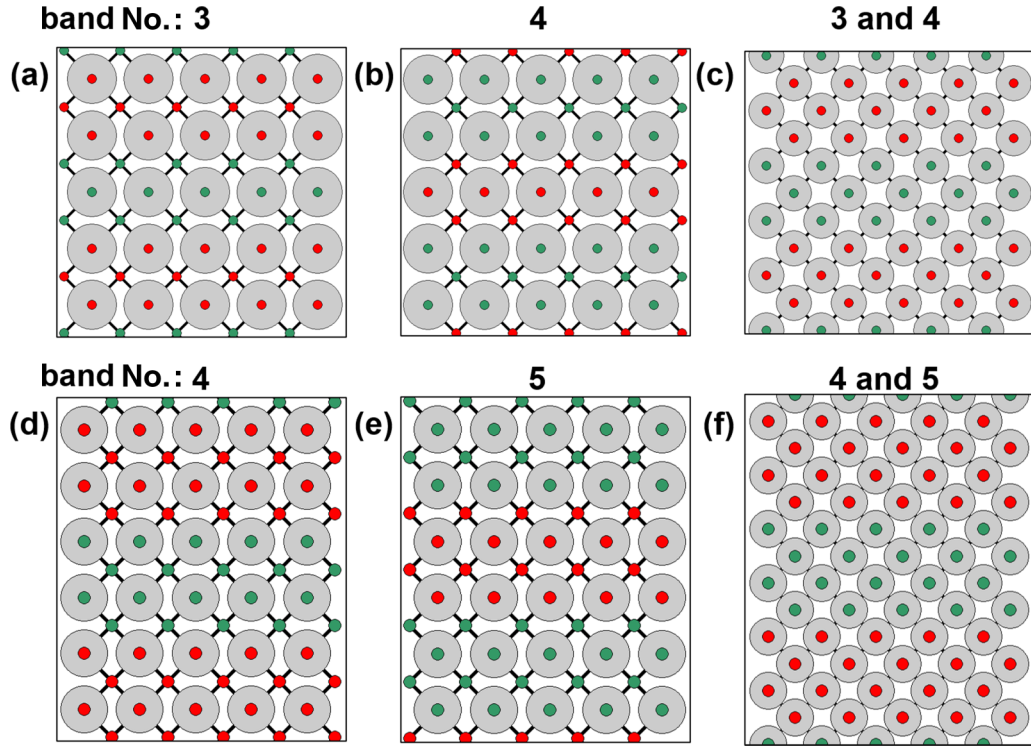
FIG. 10. The wave functions of the partial FB in DSL of $N = 6$ along M-X in Fig. 3(c) [(a) to (c)] and $N = 8$ along the k path of Γ-Y in Fig. 3(d) [(d) to (e)] with band index 3 (a), 4 (b), and all FBs (c); 4 (d), 5 (e), and all FBs (f). The size of the gray dot indicates the magnitude of the wave function. The neighboring half N sites are indicated by the green or red colors, respectively.

Here, $k_n = \vec{k} \cdot \vec{a_n}$, and $\vec{a_1} = (\hat{x} + \hat{y})$, $\vec{a_2} = (-\hat{x} + \hat{y})$. The six eigenvalues are

$$E_{1,2}(\vec{k}) = \pm t(1 + e^{ik_1+ik_2})(e^{-ik_1} + e^{-ik_2}); \quad \text{and} \quad E_{3,4,5,6}(\vec{k}) = \pm\frac{1}{2}t(e^{-ik_1} + e^{-ik_2})(1 + e^{ik_1+ik_2} \pm \sqrt{3}\sqrt{-1 + 2e^{ik_1+ik_2} - e^{2ik_1+2ik_2}}).$$

(A4)

Note that the eigenvectors corresponding to $E_{1,2}$ are $(1, 1, 1, 1, 1, 1)^T$ and $(-1, 1, -1, 1, -1, 1)^T$, which means the eigenstates are contributed equally by each sites, as shown in Fig. 4(a). The other eigenvectors are too complicated to be listed.

The TB Hamiltonian for DSL of $N = 4$ without on-site energy difference is

$$H = t * \begin{pmatrix} 0 & e^{-ik_1} + e^{-ik_2} & 0 & e^{ik_1} + e^{ik_2} \\ e^{ik_1} + e^{ik_2} & 0 & e^{-ik_1} + e^{-ik_2} & 0 \\ 0 & e^{ik_1} + e^{ik_2} & 0 & e^{-ik_1} + e^{-ik_2} \\ e^{-ik_1} + e^{-ik_2} & 0 & e^{ik_1} + e^{ik_2} & 0 \end{pmatrix},$$

(A5)

which gives four bands,

$$E_{1,2}(\vec{k}) = \pm t(e^{-ik_1} + e^{-ik_2})(1 + e^{ik_1+ik_2}); \quad \text{and} \quad E_{3,4}(\vec{k}) = \pm it(e^{-ik_1} + e^{-ik_2})(e^{ik_1+ik_2} - 1).$$

(A6)

The corresponding eigenvectors are $(1, 1, 1, 1)^T$, $(-1, 1, -1, 1)^T$, $(-i, -1, i, 1)^T$, and $(i, -1, -i, 1)^T$, which means the eigenstates are contributed equally by each site, as shown in Fig. 5(a). With on-site energy difference, the analytical solutions to eigenvalues and eigenvectors are complicated and are not listed.

APPENDIX B: SQUARE LATTICE AND BAND STRUCTURE

The eigenvalue for the simple square lattice [Fig. 9(a)] is $E(\vec{k}) = 2t(\cos k_x + \cos k_y)$. Here, $k_{x,y} = \vec{k} \cdot \vec{a_{x,y}}$, and $\vec{a_x} = \hat{x}$, $\vec{a_y} = \hat{y}$. The band structure is shown in Fig. 9(c), in which there is a partial flat band along the k path of X-Y with k_x and k_y satisfying the phase cancellation condition of
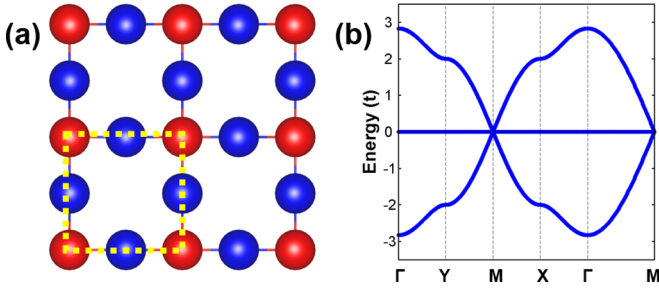
FIG. 11. (a) The Lieb lattice. The dashed square indicates the unit cell. (b) The band structure of Lieb lattice.

$|k_x \pm k_y| = \pi$. Then it can be derived that $\cos k_y = -\cos k_x$, which leads to the partial FB along X-Y.

APPENDIX C: WAVE FUNCTION OF PARTIAL FLAT BAND

In the band structure of lattice of $N = 6$ without on-site energy difference, there is a partial FB with degeneracy of 2 along M-X in Fig. 3(c). The band index for FBs are 3 and 4. The corresponding wave functions are shown in Figs. 10(a) and 10(b), respectively. One FB is contributed by half N sites, and the other FB is contributed by the other half N sites. Overall, all the sites contribute equally to the FBs, as indicated by the wave function in Fig. 10(c). Figures 10(d) to 10(f) illustrate the wave functions of the partial FB in the lattice of $N = 8$ along the k path of Γ-Y in Fig. 3(d). The same finding is obtained as that for $N = 8$.

APPENDIX D: LIEB LATTICE AND BAND STRUCTURE

The Lieb lattice is shown in Fig. 11(a), which is the derivative DSL of $N = 2$. The corner and edge sites are indicated by the red and blue colors. Without on-site energy difference of corner and edge sites, the band structure of a Lieb lattice features Dirac cones intersected by a flat band, as shown in Fig. 11(b).

APPENDIX E: TB HAMILTONIANS FOR DERIVATIVE DSLs

The Hamiltonian for derivative DSL of $N = 3$ without on-site energy difference is

$$H = t * \begin{pmatrix} 0 & e^{ik_x} & e^{-ik_x} & e^{ik_y} & 0 & e^{-ik_y} & 0 \\ e^{-ik_x} & 0 & e^{ik_x} & 0 & 0 & 0 & e^{-ik_y} \\ e^{ik_x} & e^{-ik_x} & 0 & 0 & e^{ik_y} & 0 & 0 \\ e^{-ik_y} & 0 & 0 & 0 & e^{-ik_x} & e^{ik_y} & 0 \\ 0 & 0 & e^{-ik_y} & e^{ik_x} & 0 & 0 & 0 \\ e^{ik_y} & 0 & 0 & e^{-ik_y} & 0 & 0 & e^{ik_x} \\ 0 & e^{ik_y} & 0 & 0 & 0 & e^{-ik_x} & 0 \end{pmatrix}. \tag{E1}$$

Here, $k_{x,y} = \vec{k} \cdot \overrightarrow{a_{x,y}}$, and $\overrightarrow{a_x} = \hat{x}$, $\overrightarrow{a_y} = \hat{y}$. It has one eigenvalue which equals to 0, and the corresponding eigenvector is,

$$\Psi_0(\vec{k}) = Norm(-e^{ik_x - ik_y} \quad 0 \quad 0 \quad 0 \quad e^{i2k_x - i2k_y} \quad 0 \quad 1)^T. \tag{E2}$$

Norm is the normalization factor.
The Hamiltonian for derivative DSL of $N = 4$ without on-site energy difference is

$$H = t * \begin{pmatrix} 0 & e^{ik_x} & 0 & e^{-ik_x} & e^{ik_y} & 0 & 0 & 0 & 0 & 0 & e^{-ik_y} & 0 & 0 \\ e^{-ik_x} & 0 & e^{-ik_x} & 0 & 0 & 0 & 0 & 0 & 0 & 0 & 0 & e^{-ik_y} & 0 \\ 0 & e^{-ik_x} & 0 & e^{ik_x} & 0 & e^{ik_y} & 0 & 0 & 0 & 0 & 0 & 0 & e^{-ik_y} \\ e^{ik_x} & 0 & e^{-ik_x} & 0 & 0 & 0 & e^{ik_y} & 0 & 0 & 0 & 0 & 0 & 0 \\ e^{-ik_y} & 0 & 0 & 0 & 0 & 0 & e^{-ik_x} & e^{ik_y} & 0 & 0 & 0 & 0 & 0 \\ 0 & 0 & e^{-ik_y} & 0 & 0 & 0 & e^{ik_x} & 0 & 0 & 0 & 0 & 0 & 0 \\ 0 & 0 & 0 & e^{-ik_y} & e^{-ik_x} & e^{-ik_x} & 0 & 0 & 0 & e^{ik_y} & 0 & 0 & 0 \\ 0 & 0 & 0 & 0 & e^{ik_y} & 0 & 0 & 0 & e^{ik_x} & e^{-ik_x} & e^{ik_y} & 0 & 0 \\ 0 & 0 & 0 & 0 & 0 & 0 & 0 & e^{-ik_x} & 0 & 0 & 0 & e^{ik_y} & 0 \\ 0 & 0 & 0 & 0 & 0 & 0 & 0 & e^{-ik_y} & e^{ik_x} & 0 & 0 & 0 & 0 \\ e^{ik_y} & 0 & 0 & 0 & 0 & 0 & 0 & e^{-ik_y} & 0 & 0 & 0 & e^{ik_x} & 0 \\ 0 & e^{ik_y} & 0 & 0 & 0 & 0 & 0 & 0 & e^{-ik_y} & 0 & e^{-ik_x} & 0 & e^{ik_x} \\ 0 & 0 & e^{ik_y} & 0 & 0 & 0 & 0 & 0 & 0 & 0 & 0 & e^{-ik_x} & 0 \end{pmatrix}, \tag{E3}$$
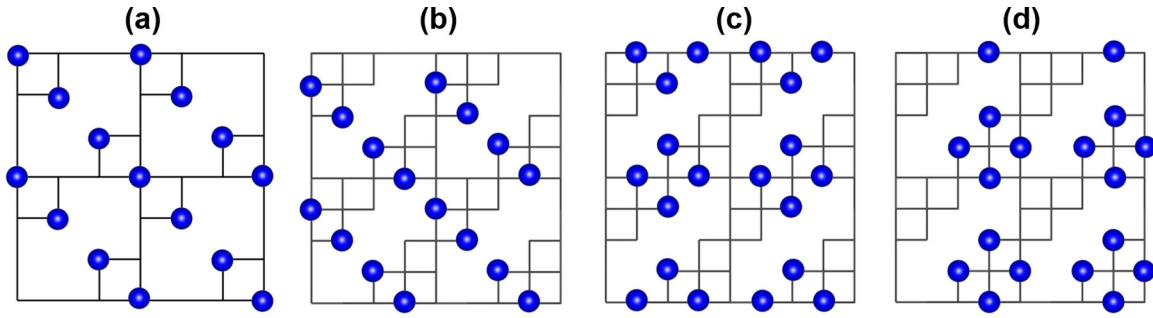
FIG. 12. The blue sites contributed to the FBs in a 2-by-2 super lattice of (a) $N = 3$, (b)–(d) $N = 4$. The black network indicates the derivative DSL.

which gives three eigenvalues that equal to 0, and the corresponding eigenvectors are

$$\Psi_{0,1}(\vec{k}) = Norm(0 \quad 0 \quad 0 \quad -e^{ik_x - ik_y} \quad 0 \quad e^{2ik_x - 2ik_y} \quad 0 \quad 0 \quad -e^{-ik_x + ik_y} \quad 0 \quad 1 \quad 0 \quad 0)^T,$$

$$\Psi_{0,2}(\vec{k}) = Norm(0 \quad -e^{ik_x - ik_y} \quad 0 \quad e^{3ik_x - ik_y} \quad 0 \quad -e^{4ik_x - 2ik_y} \quad 0 \quad 0 \quad 0 \quad 0 \quad 0 \quad 0 \quad 1)^T,$$

$$\text{and } \Psi_{0,3}(\vec{k}) = Norm(0 \quad 0 \quad 0 \quad e^{2ik_y} \quad -e^{-ik_x + ik_y} \quad -e^{ik_x + ik_y} \quad 0 \quad 0 \quad 0 \quad 1 \quad 0 \quad 0 \quad 0)^T. \tag{E4}$$

The FB of $N = 3$ lattice is only contributed by the diagonal sites of equal spacing. Similarly, the diagonal sites of $N = 4$ lattice contribute to one FB, while the other two FBs come from the four windmill-shaped sites, which also locate along the equal-spaced chains, as shown in Fig. 12.

---

[1] Z. Liu, Z. F. Wang, J. W. Mei, Y. S. Wu, and F. Liu, Phys. Rev. Lett. **110**, 106804 (2013).

[2] Z. F. Wang, Z. Liu, and F. Liu, Phys. Rev. Lett. **110**, 196801 (2013).

[3] Z. F. Wang, N. Su, and F. Liu, Nano Lett. **13**, 2842 (2013).

[4] C. L. Kane and E. J. Mele, Phys. Rev. Lett. **95**, 226801 (2005).

[5] C. L. Kane and E. J. Mele, Phys. Rev. Lett. **95**, 146802 (2005).

[6] P. R. Wallace, Phys. Rev. **71**, 622 (1947).

[7] K. S. Novoselov, A. K. Geim, S. V. Morozov, D. Jiang, Y. Zhang, S. V. Dubonos, I. V. Grigorieva, and A. A. Firsov, Science **306**, 666 (2004).

[8] W. Jiang, M. Kang, H. Huang, H. Xu, T. Low, and F. Liu, Phys. Rev. B **99**, 125131 (2019).

[9] C. C. Lee, A. Fleurence, Y. Yamada-Takamura, and T. Ozaki, Phys. Rev. B **100**, 045150 (2019).

[10] S. Zhang, M. Kang, H. Huang, W. Jiang, X. Ni, L. Kang, S. Zhang, H. Xu, Z. Liu, and F. Liu, Phys. Rev. B **99**, 100404(R) (2019).

[11] Z. Liu, F. Liu, and Y. S. Wu, Chin. Phys. B **23**, 077308 (2014).

[12] X. Ni, Y. Zhou, G. Sethi, and F. Liu, Phys. Chem. Chem. Phys. **22**, 25827 (2020).

[13] E. Tang, J. W. Mei, and X. G. Wen, Phys. Rev. Lett. **106**, 236802 (2011).

[14] X. Ni, W. Jiang, H. Huang, K. H. Jin, and F. Liu, Nanoscale **10**, 11901 (2018).

[15] Z. F. Wang, K. Jin, and F. Liu, WIREs Comput. Mol. Sci. **7**, e1304 (2017).

[16] M. Zhou, W. Ming, Z. Liu, Z. Wang, P. Li, and F. Liu, Proc. Natl. Acad. Sci. USA **111**, 14378 (2014).

[17] B. Pal and K. Saha, Phys. Rev. B **97**, 195101 (2018).

[18] T. Mizoguchi, M. Maruyama, S. Okada, and Y. Hatsugai, Phys. Rev. Mater. **3**, 114201 (2019).

[19] T. Mizoguchi, Y. Kuno, and Y. Hatsugai, Phys. Rev. A **102**, 033527 (2020).

[20] X. Ni, H. Huang, and F. Liu, Phys. Rev. B **101**, 125114 (2020).

[21] M. E. Lines, Phys. Rev. B **9**, 3927 (1974).

[22] M. Holzmann and S. Moroni, Phys. Rev. Lett. **124**, 206404 (2020).

[23] B. Monserrat, Phys. Rev. B **93**, 100301(R) (2016).

[24] L. Pietronero and S. Strassler, EPL **18**, 627 (1992).

[25] See Supplemental Material at http://link.aps.org/supplemental/10.1103/PhysRevB.102.235117 for supporting figures.

[26] F. Liu, S. N. Khanna, and P. Jena, Phys. Rev. B **42**, 976 (1990).

[27] C. Zhang, H. Huang, X. Ni, Y. Zhou, L. Kang, W. Jiang, H. Chen, J. Zhong, and F. Liu, Nanoscale **10**, 16759 (2018).

[28] A. Bhattacharya and B. Pal, Phys. Rev. B **100**, 235145 (2019).

[29] X. Mao, J. Liu, J. Zhong, and R. A. Römer, Physica E: Low Dimens. Syst. Nanostruct. **124**, 114340 (2020).

[30] W. Jiang, H. Huang, and F. Liu, Nat. Commun. **10**, 2207 (2019).

[31] D. L. Bergman, C. Wu, and L. Balents, Phys. Rev. B **78**, 125104 (2008).

[32] S. Mukherjee, A. Spracklen, D. Choudhury, N. Goldman, P. Öhberg, E. Andersson, and R. R. Thomson, Phys. Rev. Lett. **114**, 245504 (2015).

[33] Y. Zong, S. Xia, L. Tang, D. Song, Y. Hu, Y. Pei, J. Su, Y. Li, and Z. Chen, Opt. Express **24**, 8877 (2016).

[34] B. Real, C. Cantillano, D. López-González, A. Szameit, M. Aono, M. Naruse, S.-J. Kim, K. Wang, and R. A. Vicencio, Sci. Rep. **7**, 15085 (2017).

[35] S. Xia, A. Ramachandran, S. Xia, D. Li, X. Liu, L. Tang, Y. Hu, D. Song, J. Xu, D. Leykam, S. Flach, and Z. Chen, Phys. Rev. Lett. **121**, 263902 (2018).